



Power Quality Improvement Through Backstepping Super-Twisting Control of a DFIG-Based Dual Rotor Wind Turbine System Under Grid Voltage Drop

Adil Yahdou¹ · Abdelkadir Belhadj Djilali¹ · Elhadj Bounadja¹ · Zinelaabidine Boudjema¹

Received: 6 August 2023 / Accepted: 28 December 2023 / Published online: 30 January 2024
© King Fahd University of Petroleum & Minerals 2024

Abstract

The stator field-oriented control (SFOC) strategy, utilizing classical proportional-integral (PI) regulators for the doubly fed induction generator (DFIG) within a dual rotor wind turbine (DRWT) system, encounters several significant challenges. These challenges encompass undesirable fluctuations in stator active and reactive powers, the occurrence of a coupling effect in specific scenarios, and a lack of robustness. Moreover, the conventional SFOC demonstrates suboptimal performance in the presence of grid voltage drop scenarios. To address these issues, this study proposes the application of a backstepping super-twisting control (BSTC) strategy. The design of the controller involves integrating a super-twisting algorithm (STA) term into the control law of the classical backstepping control (BC) approach. The MATLAB simulation tests conducted on a 1500 KW DFIG-based DRWT system illustrate the clear superiority of the proposed BSTC over conventional SFOC, BC, and some previously published control methods. In the reference tracking test, the results indicate a significant reduction in the total harmonic distortion (THD) value of the stator current by 57.14% compared to SFOC and by 33.33% compared to BC. Additionally, the BSTC technique, in the same test, also reduces the steady-state error (SSE) for active power by 60% and 28.57% compared to SFOC and BC, respectively. Concerning reactive power, the proposed BSTC strategy decreases SSE by percentages estimated at 56.25% and 12.5%, respectively, compared to SFOC and BC. The computed percentages illustrate the substantial superiority of the suggested controller in enhancing power system characteristics and elevating the quality of energy.

Keywords Stator field oriented control · Dual rotor wind turbine · Super-twisting algorithm · Backstepping control · Grid voltage drop scenarios · DFIG

1 Introduction

In the face of depleting and environmentally harmful fossil fuels like oil, gas, and coal, there has been a growing

emphasis on developing alternative energy resources. These alternatives are crucial to address environmental concerns arising from greenhouse gas emissions during the extraction of these traditional resources. Among the alternatives, renewable energies stand out, offering a cleaner way to generate electricity and reducing dependency on finite resources. However, they do come with the challenge of managing their inherent natural and occasionally unpredictable fluctuations. One promising source of clean energy is the use of variable-speed wind turbine (VSWT) systems to produce electricity, which has become increasingly competitive in terms of production costs [1, 2]. This shift is contributing significantly to reducing greenhouse gas emissions.

A single rotor wind turbine (SRWT), which has one horizontal axis and three blades, has been commonly used to produce electrical energy. However, various other types of wind turbines, such as the DRWT, have been proposed.

✉ Adil Yahdou
a.yahdou@univ-chlef.dz
Abdelkadir Belhadj Djilali
a.belhadjdjilali@univ-chlef.dz
Elhadj Bounadja
e.bounadja@univ-chlef.dz
Zinelaabidine Boudjema
z.boudjema@univ-chlef.dz

¹ Department of Electrical Engineering, Faculty of Technology, Laboratoire Génie Electrique et Energies Renouvelables (LGEER), Hassiba Benbouali University of Chlef, Chlef, Algeria



Among its advantages are suitability for low wind speeds and an increase in the production of electrical energy compared to the SRWT [3–5]. The design of the DRWT consists of two turbines (an auxiliary turbine (AT) and a main turbine (MT)).

Currently, the VSWT employing DFIG technology is the most popular choice [6, 7]. Its primary advantage lies in the sizing of its three-phase static converters, namely the grid side converter (GSC) and rotor side converter (RSC), for only a portion of the generator nominal power. This configuration leads to substantial economic benefits compared to other electrical machines, such as permanent magnet synchronous generators (PMSG). The DFIG permits operation within a speed range of $\pm 30\%$ around the synchronism speed, which enables downsizing of the static converters. These converters are connected between the electrical network and the rotor winding of the generator, making the system more efficient and compact.

The unbalanced grid voltage scenario, resulting from voltage drop in one or more phases, causes numerous problems in the wind turbine system based on DFIG. These problems include significant undulations in electromagnetic torque and stator powers. Additionally, there are high-frequency components in rotor currents that can lead to winding losses and excessive shaft stress [8]. In the literature, several research studies have been presented to address these issues. For instance, injecting sinusoidal currents for grid-side converter with only positive-sequence components at the point of common coupling with the grid [9], using adaptive PI regulators based on neural network (NN) [10], applying the sliding mode control (SMC) algorithm [11], and implementing model predictive control (MPC) [12].

To control the stator powers of the DFIG, a vector control (VC) approach is commonly employed. VC is typically divided into two methods: stator voltage orientation control (SVOC) and SFOC [13, 14]. In both methods, PI controllers are used to regulate the reactive and active powers of the generator by adjusting d - q rotor currents. Despite its widespread use in wind turbine systems, VC has shown some limitations in terms of robustness, mainly attributed to the use of this type of controller.

Backstepping control (BC) is one of the nonlinear control methods, which is proposed to improve the VC strategy [15]. The concept of dividing entire systems into subsystems is advocated by BC, as it facilitates the derivation and computation of the desired control input. This recursive process extends outward to successive subsystems until the final optimal control is achieved. In a study referenced as [16], both classical and integral BC methods based on a decoupled control using an indirect field orientation strategy were employed for speed regulation of a three-phase induction motor (IM). The classical BC methods resulted in fluctuations in the stator current of the IM and a slight steady-state error between the

desired and actual rotor speed of the IM. However, the integral BC method improved robustness despite the presence of model uncertainties and ensured the global stability of the system. A basic BC method might not effectively reject disturbances and guarantee better robustness. Various robust BC strategies have been explored in the literature. For instance, in [17], a robust adaptive BC strategy was utilized for mobile robotic manipulators, demonstrating superior robustness and tracking performance compared to a classical proportional integral and derivative (PID) regulator. In spite of employing all these BC methods, complete suppression of external or internal disturbances is not achieved, resulting in uncertain robustness in certain scenarios.

The sliding mode control (SMC) is another nonlinear control method, which is widely used [18]. While this technique has exhibited great efficiency and robustness in the control of electrical drives, its usage has been limited due to the presence of undesirable chattering phenomenon caused by the discontinuous part of the control law. To mitigate the impact of this phenomenon, several solutions have been presented and proposed in the literature. These include the adoption of the boundary layer approach [19], utilization of the second-order sliding mode control (SOSMC) based on STA [20, 21], incorporation of passivity-sliding mode [22, 23], implementation of backstepping first-order sliding mode [24, 25], utilization of H_∞ sliding mode [26], and application of sliding mode predictive control [27, 28]. Each of these strategies mentioned above varies in terms of their underlying principles, level of complexity, ease of implementation, susceptibility to changes in system parameters, and cost.

In this research paper, a newly introduced control method called “backstepping super-twisting control” is adopted to enhance robustness and minimize the chattering issue. This approach, introduced in reference [29], has demonstrated promising outcomes, particularly in the speed control of a three-phase squirrel cage IM. Hence, it will be implemented as the chosen control strategy for this study.

The achievements of this study can be outlined as follows:

- A new controller was designed for the control of active and reactive power in the DFIG-based DRWT system.
- Formulation of the proposed controller, integrating elements from BC and STA, hereby referred to as the backstepping super-twisting controller (BSTC).
- A thorough performance evaluation was conducted, comparing SFOC, BC, and the proposed BSTC for the control of reactive and active power in the DFIG-based DRWT system under varying conditions, including extreme parameter variations and grid voltage drop.
- Improved the robustness and reduced the total harmonic distortion (THD) value of the stator current. Additionally, decreased the steady-state error (SSE) for the reactive and active power control of the generator.

The rest of the paper is organized as follows: in Sects. 2 and 3, the DRWT and DFIG models are presented. In Sect. 4, the SFOC strategy of the DFIG is explained. The proposed BSTC technique is elucidated in Sect. 5. Section 6 presents the results and their discussion. Finally, in Sect. 7, the paper’s conclusions are presented.

2 DRWT model

The DRWT is a type of turbine that has appeared recently and has provided satisfactory results, as it helps to stabilize the generating system and reduce disturbances. Additionally, it increases the value of the mechanical power gained from the wind and is not affected by the wind generated by other turbines in wind farms.

The aerodynamic torques of the MT (T_M) and AT (T_A) are given in the following equations [30]:

$$T_M = \frac{\rho \cdot \pi \cdot R_M^5 \cdot C_p \cdot \omega_M^2}{2 \cdot \lambda_M^3} \tag{1}$$

$$T_A = \frac{\rho \cdot \pi \cdot R_A^5 \cdot C_p \cdot \omega_A^2}{2 \cdot \lambda_A^3} \tag{2}$$

where λ_M and λ_A are the tip speed ratio of the MT and AT. R_M and R_A are the blade radius of the MT and AT. ω_M and ω_A are the mechanical speed of the MT and AT. ρ is the air density.

The power coefficient (C_p) can be calculated as the following equation [31]:

$$C_p(\lambda, \beta) = 0.0068 \lambda + 0.517 \left(\frac{116}{\lambda_i} - 0.4 \beta - 5 \right) \cdot e^{-\frac{21}{\lambda_i}}$$

$$\frac{1}{\lambda_i} = -\frac{0.035}{\beta^3 + 1} + \frac{1}{\lambda + 0.08\beta} \tag{3}$$

where β is pitch angle.

Tip speed ratios for the AT and MT are given by the following equations:

$$\lambda_A = \frac{\omega_A \cdot R_A}{V_1} \tag{4}$$

$$\lambda_M = \frac{\omega_M \cdot R_M}{V_M} \tag{5}$$

3 DFIG model

The Park model of DFIG is given by [32–35]:

$$\begin{cases} V_{qs} = R_s I_{qs} + \frac{d}{dt} \phi_{qs} + \omega_s \phi_{ds} \\ V_{ds} = R_s I_{ds} + \frac{d}{dt} \phi_{ds} - \omega_s \phi_{qs} \\ V_{qr} = R_r I_{qr} + \frac{d}{dt} \phi_{qr} + \omega_r \phi_{dr} \\ V_{dr} = R_r I_{dr} + \frac{d}{dt} \phi_{dr} - \omega_r \phi_{qr} \end{cases}, \begin{cases} \phi_{qs} = L_s I_{qs} + M I_{qr} \\ \phi_{ds} = L_s I_{ds} + M I_{dr} \\ \phi_{qr} = L_r I_{qr} + M I_{qs} \\ \phi_{dr} = L_r I_{dr} + M I_{ds} \end{cases} \tag{6}$$

where I_{qr}, I_{dr}, I_{qs} and I_{ds} are the rotor and stator currents in the d - q reference frame; V_{qr}, V_{dr}, V_{qs} and V_{ds} are the rotor and stator voltages in the d - q reference frame; $\phi_{qr}, \phi_{dr}, \phi_{qs}$ and ϕ_{ds} are rotor and stator flux in the d - q reference frame; M, L_r and L_s are respectively the mutual inductance, the inductance on the rotor and the inductance on the stator. R_r and R_s are respectively the resistances of the rotor and stator windings; The rotor and stator angular velocities are linked by the following relation $\omega_s = \omega_m + \omega_r$; ω_r is the electrical pulsation of the rotor and ω_s is the stator one, while ω_m is the mechanical pulsation of the generator.

The expressions of the stator reactive power (Q_s) and active power (P_s) delivered from the DFIG are given by:

$$\begin{cases} Q_s = I_{ds} V_{qs} - I_{qs} V_{ds} \\ P_s = I_{ds} V_{ds} + I_{qs} V_{qs} \end{cases} \tag{7}$$

The mechanical equation supplements the generator’s electrical model and is given by Eq. (8).

$$T_e = T_r + J \frac{d\Omega}{dt} + f \Omega \tag{8}$$

where Ω is the mechanical rotor speed, T_r is the load torque, f is the viscous friction, and J is the inertia.

Equation (9) shows the electromagnetic torque T_e of DFIG.

$$T_e = p \frac{M}{L_s} (I_{dr} \phi_{qs} - I_{qr} \phi_{ds}) \tag{9}$$

where p is the number of pole pairs.

4 SFOC strategy

SFOC is a crucial method within the domain of renewable energy systems, specifically applied to DFIGs. SFOC involves aligning the stator flux with the rotor magnetic field, a process that optimizes the generator’s performance, leading

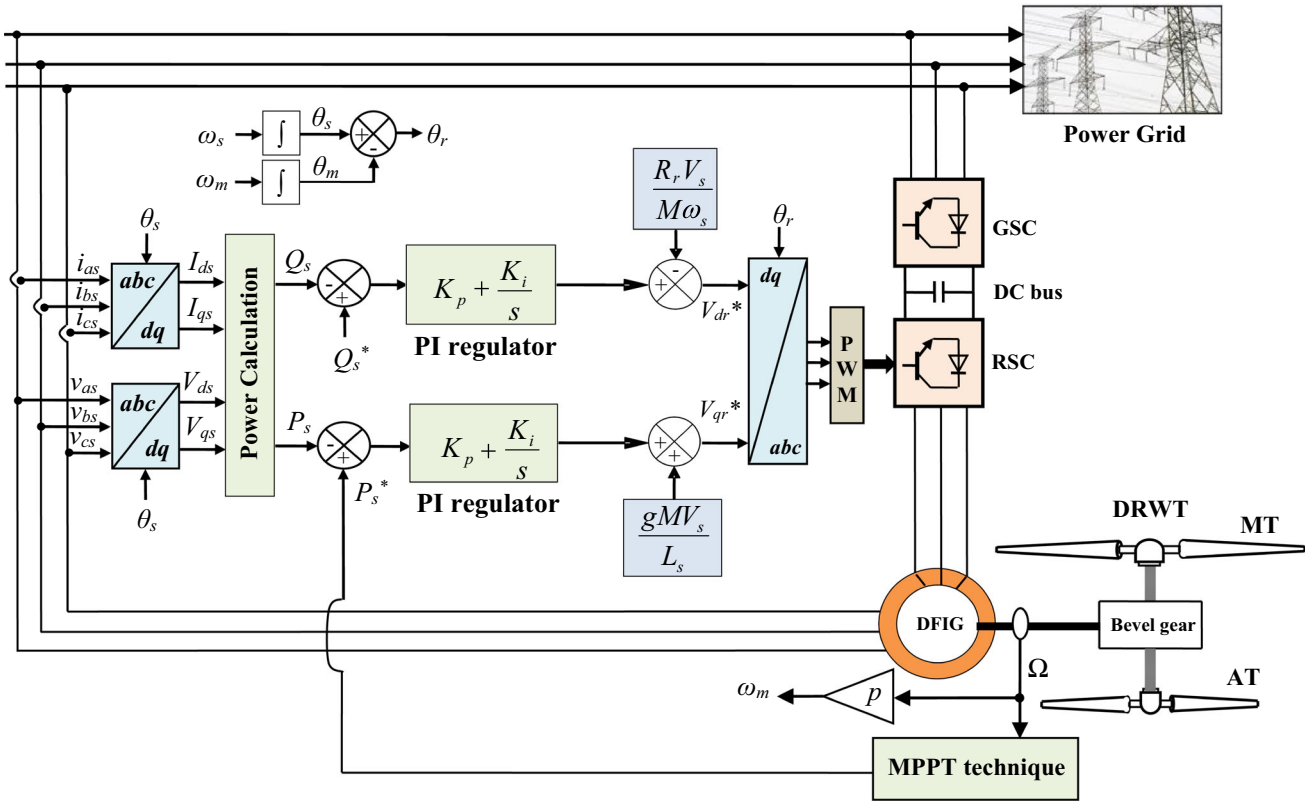


Fig. 1 Power control scheme of DRWT system based on SFOC

to improved efficiency and overall output. This control strategy allows for accurate control of both active and reactive power, ensuring the stable and reliable operation of DFIGs, especially in conditions of variable wind. With the goal of achieving decoupled stator reactive and active power control of the DFIG-based DRWT, the SFOC method will be applied. This control strategy is based on two PI regulators, as illustrated in Fig. 1.

The stator flux vector ϕ_s will be aligned along the d -axis. We will neglect the stator resistance R_s , and based on the previous Eqs. (6) and (7), we can write:

$$\phi_{qs} = 0 \quad \text{and} \quad \phi_{ds} = \phi_s \tag{10}$$

$$\begin{cases} V_{qs} = V_s = \phi_s \omega_s \\ V_{ds} = 0 \end{cases} \tag{11}$$

$$\begin{cases} I_{qs} = -\frac{M}{L_s} I_{qr} \\ I_{ds} = \frac{V_s}{\omega_s L_s} - \frac{M}{L_s} I_{dr} \end{cases} \tag{12}$$

When using Eqs. (10), (11), and (12), Eqs. (7) and (9) become:

$$\begin{cases} Q_s = \frac{V_s^2}{L_s \omega_s} - \frac{M V_s}{L_s} I_{dr} \\ P_s = -\frac{M V_s}{L_s} I_{qr} \end{cases} \tag{13}$$

$$T_e = -p \frac{M}{L_s} \phi_s I_{qr} \tag{14}$$

Posing: $g = \frac{\omega_r}{\omega_s}$ and $\sigma = 1 - \frac{M^2}{L_s L_r}$. where g and σ are the slip and the magnetic dispersion coefficient, respectively.

The derivatives of quadrature and direct rotor currents are given by [36]:

$$\begin{cases} \frac{dI_{qr}}{dt} = \frac{1}{\sigma L_r} \left[V_{qr} - R_r I_{qr} - g \omega_s \sigma L_r I_{dr} - \frac{g M V_s}{L_s} \right] \\ \frac{dI_{dr}}{dt} = \frac{1}{\sigma L_r} \left[V_{dr} - R_r I_{dr} + g \omega_s \sigma L_r I_{qr} \right] \end{cases} \tag{15}$$

The parameters of PI regulators represented in Fig. 1 are given by [37]:

$$K_i = \frac{1}{\tau_r} \frac{L_s R_r}{MV_s} \tag{16}$$

$$K_p = \frac{1}{\tau_r} \frac{L_s L_r \sigma}{MV_s} \tag{17}$$

where K_i , K_p and τ_r represent respectively the integral gain, proportional gain and response time.

To simplify the study of the application of the proposed controller, we will consider the following changes of variables: $f_1 = -R_r I_{qr} - g\omega_s \sigma L_r I_{dr} - \frac{gMV_s}{L_s}$ and $f_2 = -R_r I_{dr} + g\omega_s \sigma L_r I_{qr}$.

Equation (15) becomes:

$$\begin{cases} \frac{dI_{qr}}{dt} = \frac{1}{\sigma L_r} [V_{qr} + f_1] \\ \frac{dI_{dr}}{dt} = \frac{1}{\sigma L_r} [V_{dr} + f_2] \end{cases} \tag{18}$$

5 Proposed BSTC

The BSTC technique is a control method proposed in this paper to address several challenges, including overcoming stator power ripples, improving stator current quality, and minimizing the impact of grid voltage drop. Additionally, this control is designed to enhance the overall robustness of the system. To implement this suggested control, certain concepts or information must be provided to the conventional BC to facilitate the understanding and application of the proposed control's working principles.

5.1 Conventional BC

The backstepping approach is implemented utilizing principles from the Lyapunov stability theory, with the control law formulated through the construction of the Lyapunov function. The process of determining the control laws for the conventional controller involves following two fundamental steps:

First step: the tracking error e_1 is given by:

$$e_1 = P_s^* - P_s \tag{19}$$

The Lyapunov function V_1 is given by:

$$V_1 = \frac{1}{2} \cdot e_1^2 \tag{20}$$

The derivative of the Lyapunov function V_1 is:

$$\dot{V}_1 = e_1 \cdot \dot{e}_1 \tag{21}$$

$$\dot{e}_1 = \dot{P}_s^* - \dot{P}_s = \dot{P}_s^* + \frac{MV_s}{L_s} \cdot \dot{I}_{qr} \tag{22}$$

According to Eqs. (18), Eq. (22) becomes, when we replace the derivative of I_{qr} :

$$\dot{e}_1 = \dot{P}_s^* + \frac{MV_s}{L_s L_r \sigma} \cdot (V_{qr} + f_1) \tag{23}$$

Posing: $\psi = \frac{MV_s}{L_s L_r \sigma}$.
Equation (23) becomes:

$$\dot{e}_1 = \dot{P}_s^* + \psi \cdot (V_{qr} + f_1) \tag{24}$$

Equation (24) is replaced in Eq. (21), we obtained:

$$\dot{V}_1 = e_1 \cdot \dot{e}_1 = e_1 \cdot (\dot{P}_s^* + \psi \cdot (V_{qr} + f_1)) \tag{25}$$

The first control law of the BC is proposed to be:

$$V_{qr} = -\frac{1}{\psi} (\dot{P}_s^* + k_1 \cdot e_1) - f_1 \tag{26}$$

where: k_1 is a positive gain.

Equation (26) is replaced in Eq. (25), we obtained:

$$\dot{V}_1 = -k_1 \cdot e_1^2 \leq 0 \tag{27}$$

Second step: the tracking error e_2 is given by:

$$e_2 = Q_s^* - Q_s \tag{28}$$

The Lyapunov function V_2 is given by:

$$V_2 = V_1 + \frac{1}{2} \cdot e_2^2 \tag{29}$$

Its derivative is:

$$\dot{V}_2 = \dot{V}_1 + e_2 \cdot \dot{e}_2 \tag{30}$$

where:

$$\dot{e}_2 = \dot{Q}_s^* + \frac{MV_s}{L_s} \cdot \dot{I}_{dr} \tag{31}$$

According to Eqs. (18), Eq. (31) becomes, when we replace the derivative of I_{dr} :

$$\dot{e}_2 = \dot{Q}_s^* + \psi \cdot (V_{dr} + f_2) \tag{32}$$

Equation (32) is replaced in Eq. (30), we obtained:

$$\dot{V}_2 = \dot{V}_1 + e_2 \cdot \dot{e}_2 = \dot{V}_1 + e_2 \cdot (\dot{Q}_s^* + \psi \cdot (V_{dr} + f_2)) \quad (33)$$

The second control law of the BC is proposed to be:

$$V_{dr} = -\frac{1}{\psi}(\dot{Q}_s^* + k_2 \cdot e_2) - f_2 \quad (34)$$

where: k_2 is a positive gain.

Equation (34) is replaced in Eq. (33), we obtained:

$$\dot{V}_2 = \dot{V}_1 - k_2 \cdot e_2^2 = -k_1 \cdot e_1^2 - k_2 \cdot e_2^2 \leq 0 \quad (35)$$

Equations (35) and (27) are negative, which guarantee asymptotic stability of the system according to the Lyapunov theorem.

5.2 Conventional STA

In the field of control, STA is one of the simplest types of high-order SMC technique and the easiest to implement, as it can be applied without requiring knowledge of the mathematical form of the system under study. It can be applied directly after identifying the error. Compared with SMC, the STA technique is more robust and significantly reduces the chattering problem. The control laws of the STA are given by the following equations [20]:

$$u = u_1 + u_2 \quad (36)$$

$$u_1 = -\alpha \cdot |s|^{\frac{1}{2}} \cdot \text{sign}(s) \quad (37)$$

$$\dot{u}_2 = -\beta \cdot \text{sign}(s) \quad (38)$$

where s is the sliding surface and β, α are the positive gains.

In order to guarantee the asymptotic stability of the system, the STA control parameters α and β are selected as outlined below [20]:

$$\begin{cases} \beta > \frac{\delta(5\alpha^2 + 4\delta)}{2(\alpha - 2\delta)} \\ \alpha > 2\delta \end{cases} \quad (39)$$

where δ is a positive constants.

5.3 BSTC

The proposed BSTC technique is a modification of the conventional BC method, where the term representing a STA is added to the control laws. The goal of this technique is to enhance the quality of the energy produced by the

DFIG-based DRWT. Figure 2 represents the proposed control scheme for DRWT system based on BSTC technique.

The suggested BSTC aims to calculate the reference voltage values according to the following equations:

$$V_{qr} = -\frac{1}{\psi} \left(\dot{P}_s^* + k_1 \cdot e_1 + \alpha_1 \cdot |e_1|^{\frac{1}{2}} \cdot \text{sign}(e_1) + \int_0^t \beta_1 \cdot \text{sign}(e_1) d\tau \right) - f_1 \quad (40)$$

$$V_{dr} = -\frac{1}{\psi} \left(\dot{Q}_s^* + k_2 \cdot e_2 + \alpha_2 \cdot |e_2|^{\frac{1}{2}} \cdot \text{sign}(e_2) + \int_0^t \beta_2 \cdot \text{sign}(e_2) d\tau \right) - f_2 \quad (41)$$

where $k_1, k_2, \alpha_1, \beta_1, \alpha_2$ and β_2 are the positive gains that satisfy Eq. (39).

5.4 Stability examination of the proposed controller

In this part, our emphasis is on the essential aspect of guaranteeing the stability of control systems. The primary goal of any control system is to ensure stability and achieve optimal performance despite uncertainties and external disruptions. To comprehensively assess the stability of the control methodology presented in this research, we employ Lyapunov theory, a widely recognized mathematical framework known for providing insights into system behavior and confirming stability. This examination aims to demonstrate the effectiveness and reliability of our proposed control strategy in maintaining resilient system stability, ultimately laying the foundation for its successful implementation in practical, real-world scenarios.

The stability of the proposed control system is demonstrated as follow:

We replace the Eq. (40) in Eq. (25), we obtain:

$$\begin{aligned} \dot{V}_1 &= -k_1 \cdot e_1^2 - e_1 \\ &\cdot \left(\alpha_1 \cdot |e_1|^{\frac{1}{2}} \cdot \text{sign}(e_1) + \int_0^t \beta_1 \cdot \text{sign}(e_1) d\tau \right) \\ &= -k_1 \cdot e_1^2 - \alpha_1 \cdot |e_1|^{\frac{1}{2}} \cdot e_1 \cdot \text{sign}(e_1) \\ &\quad - \beta_1 \cdot e_1 \cdot \text{sign}(e_1) \int_0^t d\tau \\ &= -k_1 \cdot e_1^2 - \alpha_1 \cdot |e_1|^{\frac{1}{2}} \cdot e_1 \cdot \text{sign}(e_1) \\ &\quad - \beta_1 \cdot e_1 \cdot \text{sign}(e_1) \cdot t \\ &= -k_1 \cdot e_1^2 - \alpha_1 \cdot |e_1|^{\frac{1}{2}} \cdot |e_1| - \beta_1 \cdot |e_1| \cdot t \leq 0 \end{aligned} \quad (42)$$



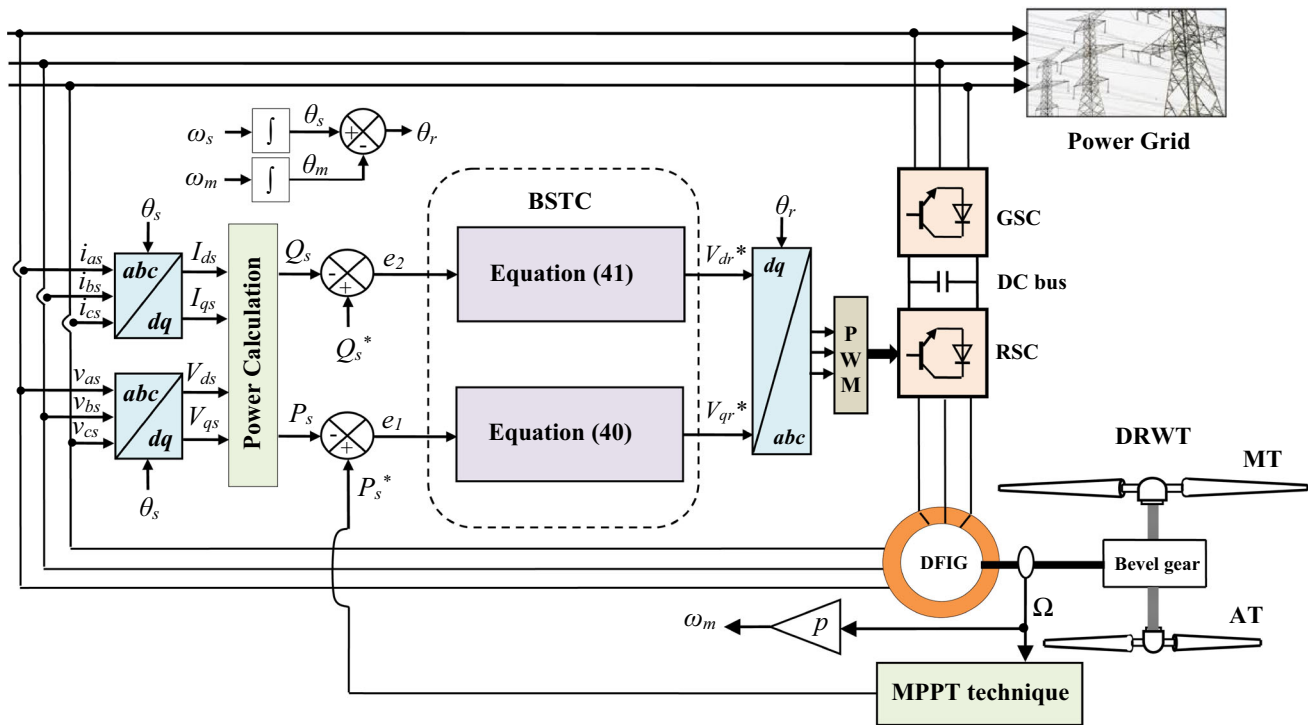


Fig. 2 Proposed control scheme for DRWT system based on BSTC

We replace the Eq. (41) in Eq. (33), we obtain:

$$\begin{aligned}
 \dot{V}_2 &= \dot{V}_1 - k_2 \cdot e_2^2 \\
 &\quad - e_2 \left(\alpha_2 \cdot |e_2|^{\frac{1}{2}} \cdot \text{sign}(e_2) + \int_0^t \beta_2 \cdot \text{sign}(e_2) d\tau \right) \\
 &= \dot{V}_1 - k_2 \cdot e_2^2 - \alpha_2 \cdot |e_2|^{\frac{1}{2}} \cdot e_2 \cdot \text{sign}(e_2) \\
 &\quad - \beta_2 \cdot e_2 \cdot \text{sign}(e_2) \int_0^t dt \\
 &= \dot{V}_1 - k_2 \cdot e_2^2 - \alpha_2 \cdot |e_2|^{\frac{1}{2}} \cdot e_2 \cdot \text{sign}(e_2) \\
 &\quad - \beta_2 \cdot e_2 \cdot \text{sign}(e_2) \cdot t \\
 &= \dot{V}_1 - k_2 \cdot e_2^2 - \alpha_2 \cdot |e_2|^{\frac{1}{2}} \cdot |e_2| \\
 &\quad - \beta_2 \cdot |e_2| \cdot t \leq 0
 \end{aligned} \tag{43}$$

Due to Eqs. (42) and (43), the stability of the proposed controller is guaranteed since the derivatives of the Lyapunov functions are negative.

6 Results and Discussion

The proposed control (BSTC) applied to the DFIG-based DRWT, as explained in Sect. 5, was simulated using MATLAB software, and the obtained results were compared to those of conventional controls.

The mechanical parameters of DRWT are as follows [38]: blade radius of the MT $R_M = 25.5$ m, blade radius of the AT $R_A = 13.2$ m, bevel gear base circle radius of the MT is $r_1 = 1$ m, bevel gear base circle radius of the AT is $r_2 = 0.5$ m, bevel gear base circle radius of the generator is $r_3 = 0.75$ m, MT inertia momentum $J_M = 1000$ kg m², and AT inertia momentum $J_A = 500$ kg m².

The parameters of the studied DFIG are as follows [32]: stator voltage $V_s = 398$ V, $R_r = 0.021$ Ω , $L_r = 0.0136$ H, $R_s = 0.012$ Ω , $L_s = 0.0137$ H, stator frequency $f_s = 50$ Hz, $M = 0.0135$ H, $p = 2$, $J = 1000$ kg m², and $f = 0.0024$ Nm/rad s⁻¹.

In this research, four tests were presented and analyzed: the first one is the reference tracking test (RTT), the second is the robustness test (RT), the third is the grid voltage drop test (GVDT), and the fourth test is the random wind speed test.

In the first, second, and third tests, we studied the performances of SFOC, BC, and BSTC under the wind speed conditions illustrated in Fig. 3.

6.1 First Test

The obtained simulation results are depicted in Figs. 4, 5, 6, 7 for this first test (RTT). As depicted in Figs. 4 and 5, for the three methods of reactive and active powers control (SFOC, BC, and BSTC), the DFIG stator powers (P_s and Q_s) follow their references (P_s^* and Q_s^*) perfectly. We notice that the

Fig. 3 Wind speed profile

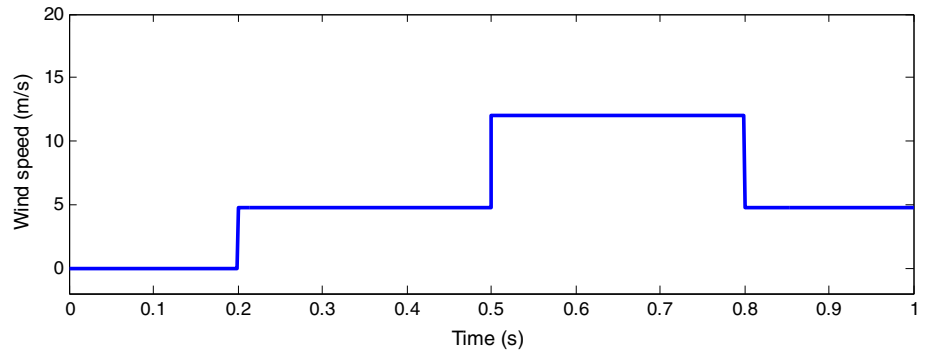


Fig. 4 Active power

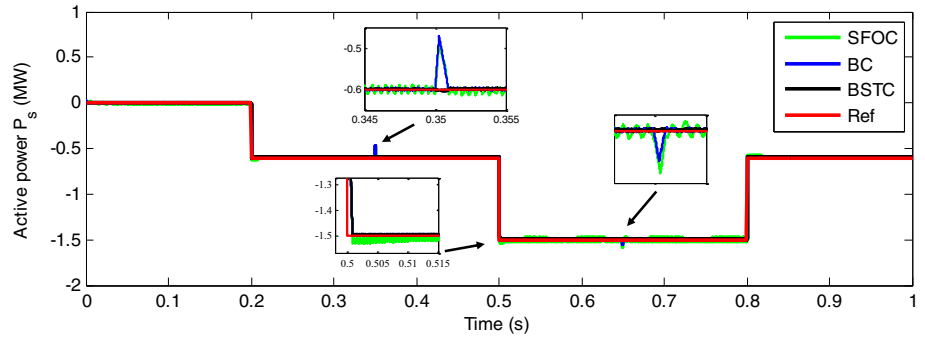


Fig. 5 Reactive power

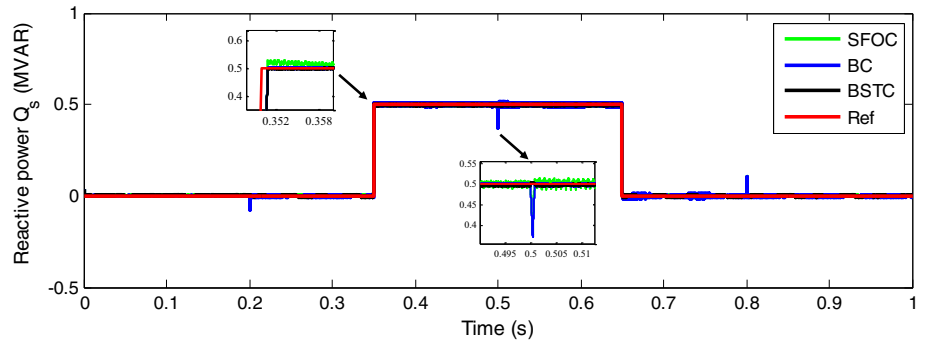


Fig. 6 Stator currents (RTT)

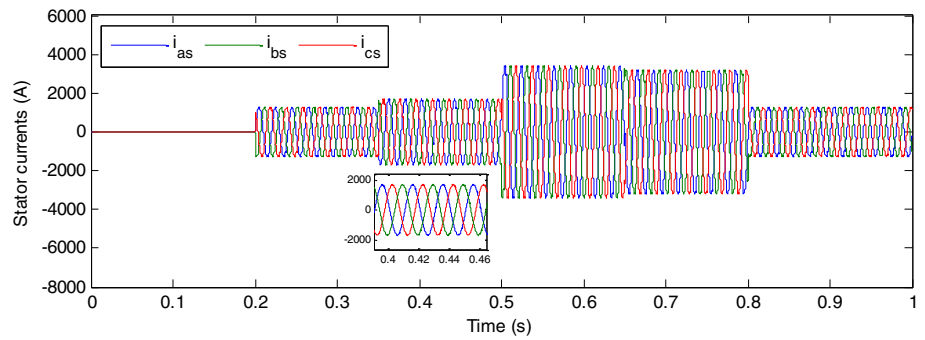
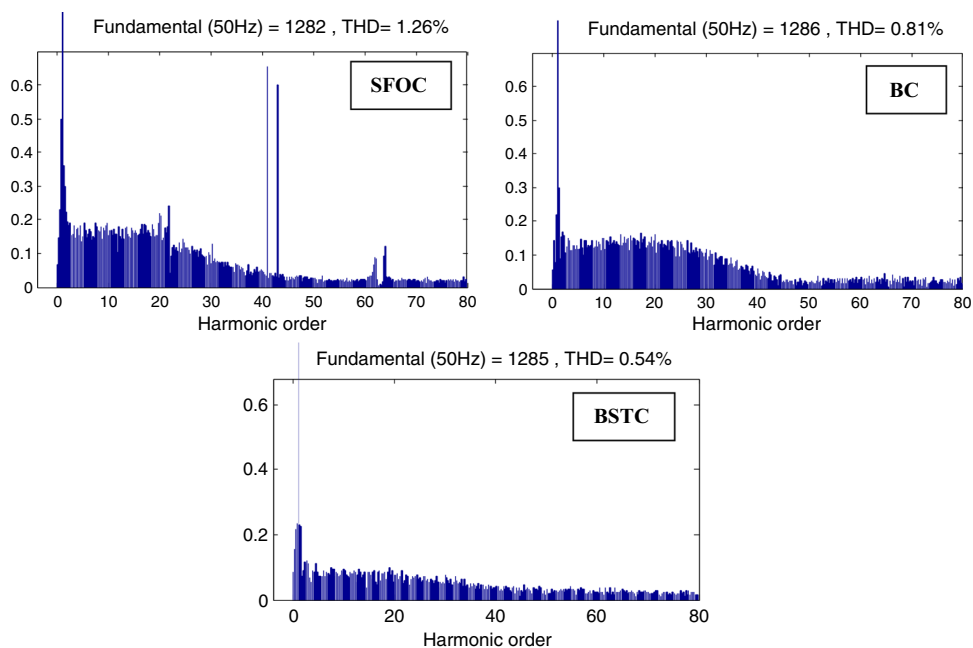


Fig. 7 THD of stator current (RTT)



stator active power reference (P_s^*) is obtained using the Maximum Power Point Tracking (MPPT) strategy, which makes the value of the stator active power (P_s) highly related to the rotation speed of the turbine. Nevertheless, we can observe a clear coupling effect between the reactive and active stator powers for SFOC and BC (seen in the active power curve at $t = 0.35$ s and $t = 0.65$ s, and in the reactive power curve at $t = 0.2$ s, $t = 0.5$ s, and $t = 0.8$ s). However, we can also notice in these Figures that the decoupling between the stator powers (P_s and Q_s) is perfectly ensured for the proposed controller.

Figure 6 depicts the simulation results of electric stator currents generated by the DFIG-based DRWT when employing the proposed BSTC. The simulation demonstrates a noticeable relationship between the variation in active power and the electric stator currents. Furthermore, the electric stator currents exhibit a well-defined sinusoidal form for this first test.

Figure 7 shows the THD (Total Harmonic Distortion) of the one-phase electric stator current (i_{as}) of the generator for the three used controls (SFOC, BC, and BSTC) for RTT. These results prove that the value of THD is minimized when we use the proposed BSTC (THD = 0.54%) compared to SFOC (THD = 1.26%) and BC (THD = 0.81%). Hence, it can be asserted that the proposed control resulted in a decrease in THD value by approximately 57.14% compared to SFOC and by 33.33% compared to BC.

The numerical results of steady-state error (SSE) for this test are represented in Table 1. From this table, the proposed control strategy provided better numerical results than the SFOC and BC. Specifically, the BSTC strategy achieved

Table 1 Values and ratios of SSE in the first test case

	P_s (MW)	Q_s (MVAR)
SFOC	0.01	0.008
BC	0.0056	0.004
BSTC	0.004	0.0035
Ratios (BSTC compared to SFOC)	60%	56.25%
Ratios (BSTC compared to BC)	28.57%	12.5%

significant reductions in SSE for active power, with percentages estimated at 60%, 28.57%, respectively, compared to the SFOC and BC.

In terms of reactive power, the proposed strategy reduced SSE by percentages estimated at 56.25%, 12.5%, respectively, compared to the SFOC and BC.

In conclusion, based on this initial test, it can be stated that BSTC performs significantly better than classical control methods (SFOC and BC).

6.2 Second Test

The robustness test involves varying the parameters of the DFIG model. Specifically, classical regulator calculations rely on transfer functions with assumed fixed parameters. However, in a real system, these parameters undergo variations due to various physical phenomena (such as inductance saturation and resistance heating). Additionally, the identification of these parameters is prone to inaccuracies stemming from the method employed and the measuring devices used.

Fig. 8 Active power

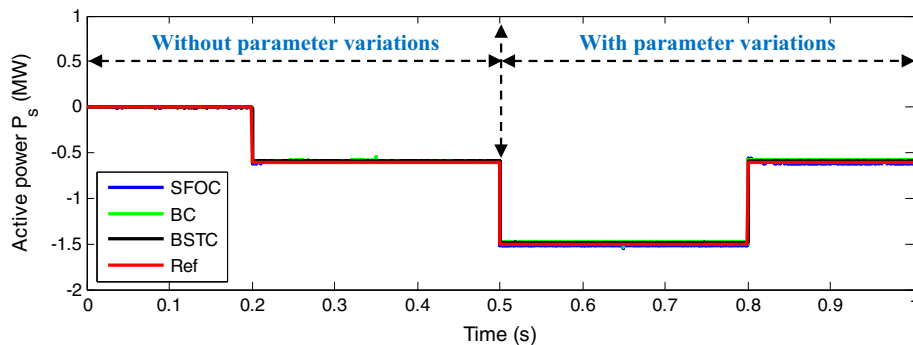


Fig. 9 Reactive power

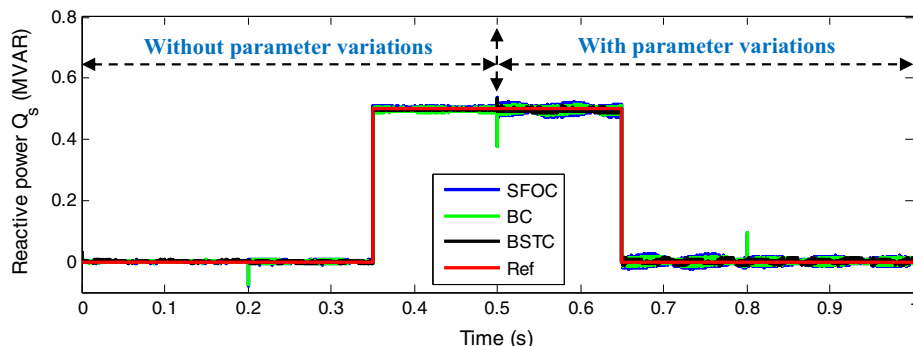
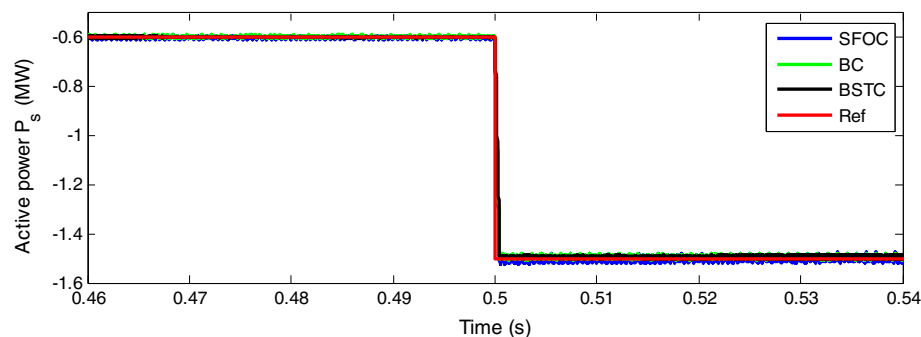


Fig. 10 Zoom (active power)



As part of testing the robustness of the studied controllers (SFOC, BC, and BSTC), we assume that the DFIG parameters are varied under severe conditions as follows:

- The value of the rotor resistance is doubled starting from 0.5 s;
- The values of stator inductance (L_s), mutual inductance (M) and rotor inductance (L_r) respectively are decreased up to 50% starting from 0.5 s.

The obtained simulation results are illustrated in Figs. 8, 9, 10, 11, 12, 13. From these results, it can be noticed that the effect of DFIG parameter variations is very clear for SFOC and BC compared to the proposed control method (BSTC), especially when zooming in on the curves of stator active and reactive power (Figs. 10 and 11). Additionally, it is noted that P_s and Q follow the references well for all control methods (Figs. 8 and 9), with a priority given to the proposed control

in terms of dynamic response. Moreover, stator power ripples are observed at the level of capacities, and these ripples are greater in the case of SFOC and BC.

Figure 12 shows the outcomes of the simulation conducted on the electric stator currents produced by the DFIG-based DRWT using the proposed BSTC. The simulation clearly illustrates a significant correlation between the variations in the electric stator currents and the stator active power. Additionally, during this second test, the electric stator currents exhibit a good sinusoidal form.

Figure 13 illustrates the THD of i_{as} of the DFIG-based DRWT during the RT. When we compare the THD values of SFOC (1.58%), BC (0.97%), and BSTC (0.58%), we can conclude that the proposed control present the best THD in this second test. Therefore, it can be stated that the implementation of the BSTC technique led to a reduction in the THD value by around 63.29% when compared to SFOC and by 40.20% when compared to BC.

Fig. 11 Zoom (reactive power)

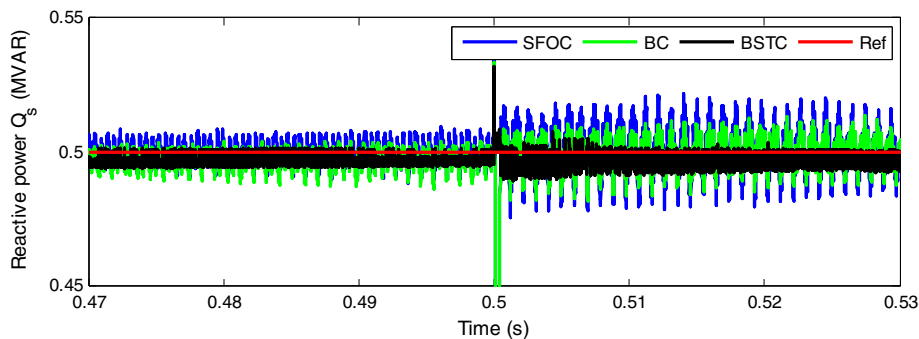


Fig. 12 Stator currents (RT)

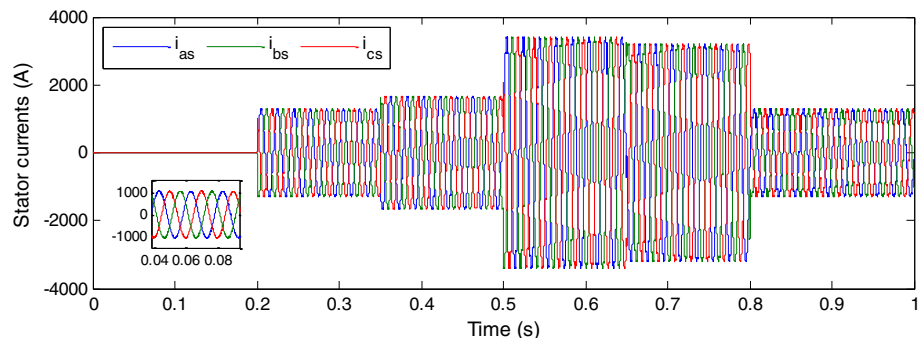


Fig. 13 THD of stator current (RT)

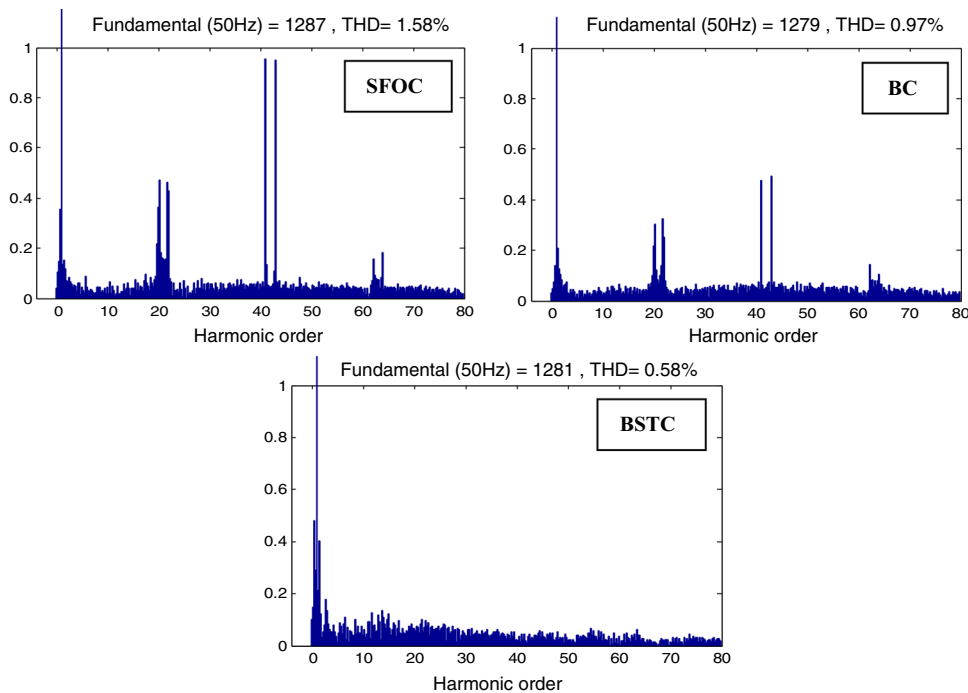


Table 2 displays the quantitative outcomes of SSE in the second test. According to the table, the suggested control approach yielded superior numerical outcomes compared to SFOC and BC. Notably, the BSTC strategy resulted in substantial decreases in SSE for active power, with percentages reaching 62.96% and 52.15% in comparison to SFOC and BC, respectively. Regarding reactive power, the proposed

strategy achieved reductions in SSE estimated at 44.73% and 30% compared to SFOC and BC, respectively.

In summary, with respect to this second test, it can be asserted that the suggested control method demonstrates greater robustness when compared to traditional control approaches.

Table 2 Values and ratios of SSE in the second test case

	P_s (MW)	Q_s (MVAR)
SFOC	0.027	0.019
BC	0.0209	0.015
BSTC	0.01	0.0105
Ratios (BSTC compared to SFOC)	62.96%	44.73%
Ratios (BSTC compared to BC)	52.15%	30%

6.3 Third Test

When a wind turbine system connected to the grid experiences a drop in grid voltage, various challenges may arise. The immediate consequence is a hindrance to the turbine's

capacity to generate electricity efficiently. A decline in grid voltage can result in diminished power quality, impacting the overall stability and dependability of the entire wind turbine system. This, in turn, can lead to decreased power output and operational efficiency in turbines, potentially resulting in economic losses. Additionally, the occurrence of grid voltage drops may activate protective measures within the turbines, leading to automatic shutdowns or restrictions in power production to prevent harm to the system. Effectively addressing these challenges necessitates the implementation of advanced control systems and grid management strategies to ensure the seamless integration of wind turbines with the grid, even amidst voltage fluctuations.

The objective of this test is to observe the behavior of the proposed control technique in response to a 15% grid voltage drop (GVD) in phase A, assumed to occur between 0.55 and

Fig. 14 Simulation result of:
a Grid voltage, b Zoom of grid voltage

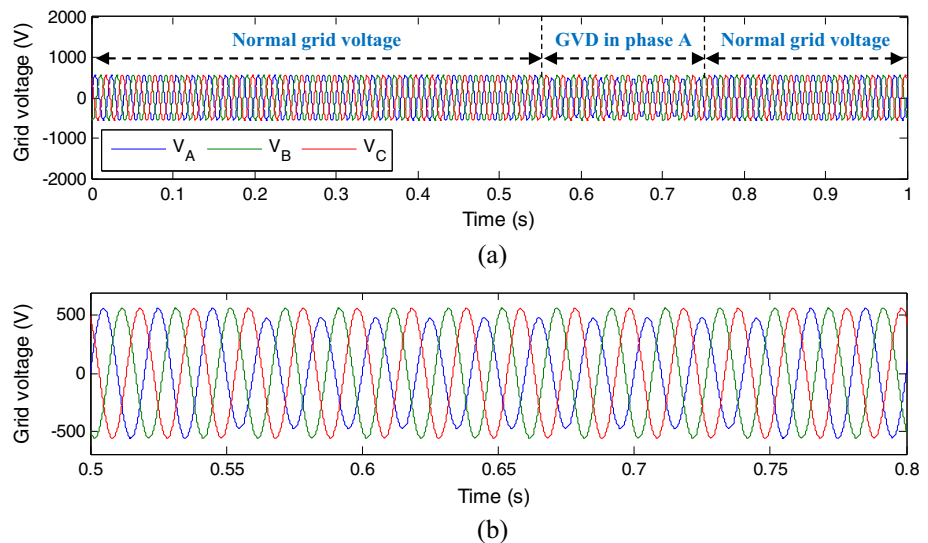


Fig. 15 Result of the electromagnetic torque

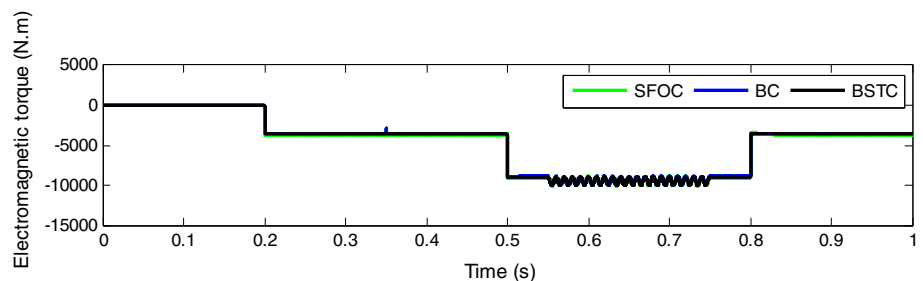


Fig. 16 Zoom (Electromagnetic torque)

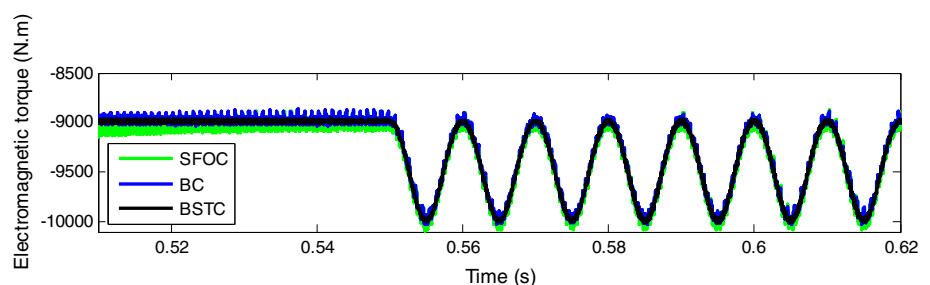


Fig. 17 THD of stator current (GVDT)

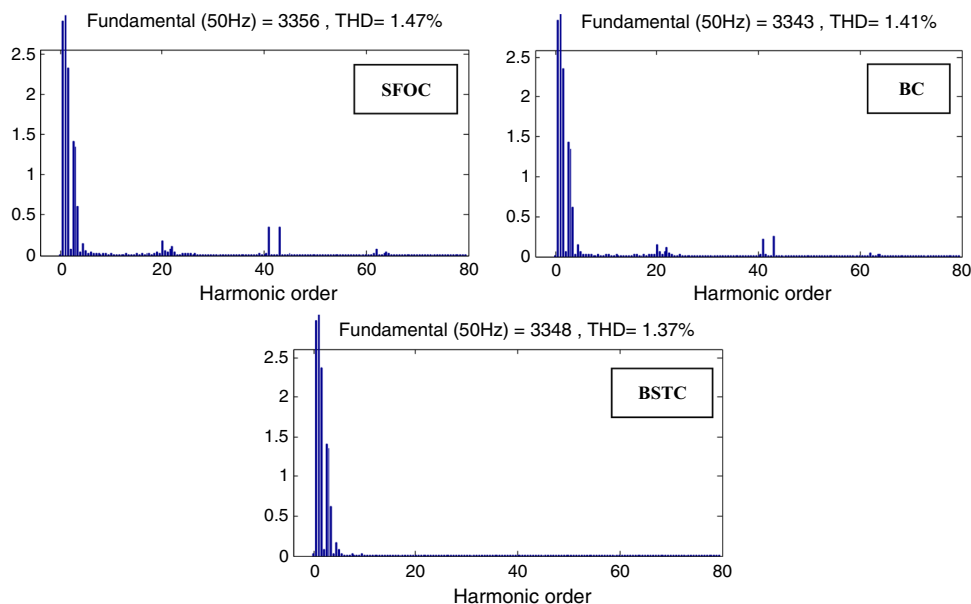
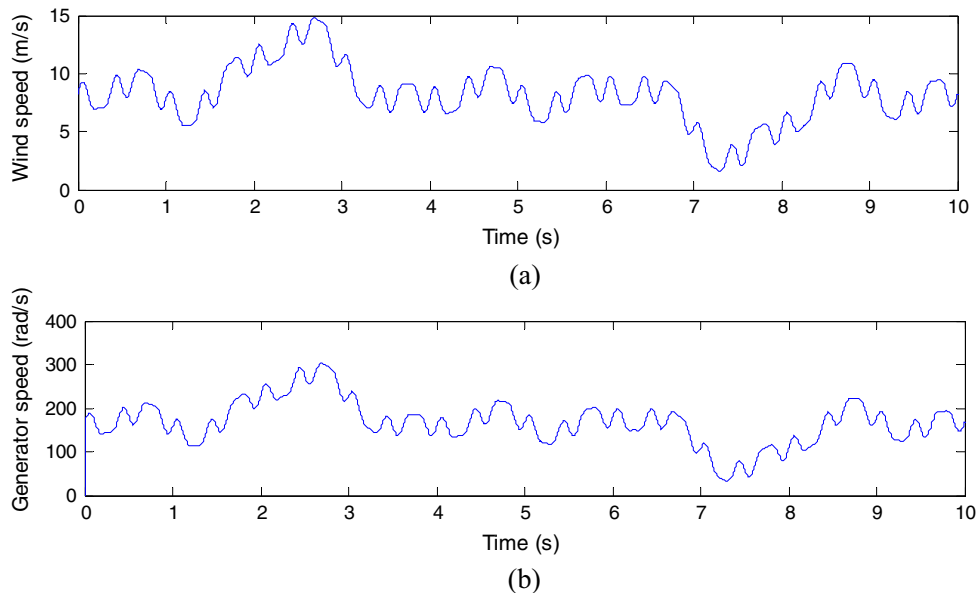


Fig. 18 Simulation results of: **a** WS profile **b** generator speed



0.75 s as illustrated in Fig. 14a and b, and compare it to other conventional controls. The simulation results for this test are depicted in Figs. 15–17.

Figures 15 and 16 depict the dynamic responses of the electromagnetic torque (T_e) of the DFIG-based DRWT during GVDT. As illustrated in these figures, the impact of GVD is evident for all studied control techniques. However, the undulations in T_e are noticeably reduced when employing the proposed control compared to other control methods.

Figure 17 illustrates the THD of i_{as} of the DFIG-based DRWT during the GVDT. From these results, it can be noticed that the effect of the grid voltage drop is very clear, resulting in significant THD values for SFOC (THD = 1.47%) and BC (THD = 1.41%), compared to the proposed

BSTC (THD = 1.37%). We can infer that, in this test, the proposed control exhibits the lowest THD of stator current value. Consequently, it can be affirmed that employing the BSTC technique resulted in a THD reduction of approximately 6.80% compared to SFOC and 2.83% compared to BC.

6.4 Fourth Test

In this fourth test, a distinct wind speed (WS) is employed, differing from the WS used in prior tests, where the WS applied was random, as depicted in Fig. 18a. Also, Fig. 18b represents the DFIG rotor speed (Ω), through this figure, it can be noticed that Ω follows the WS profile.

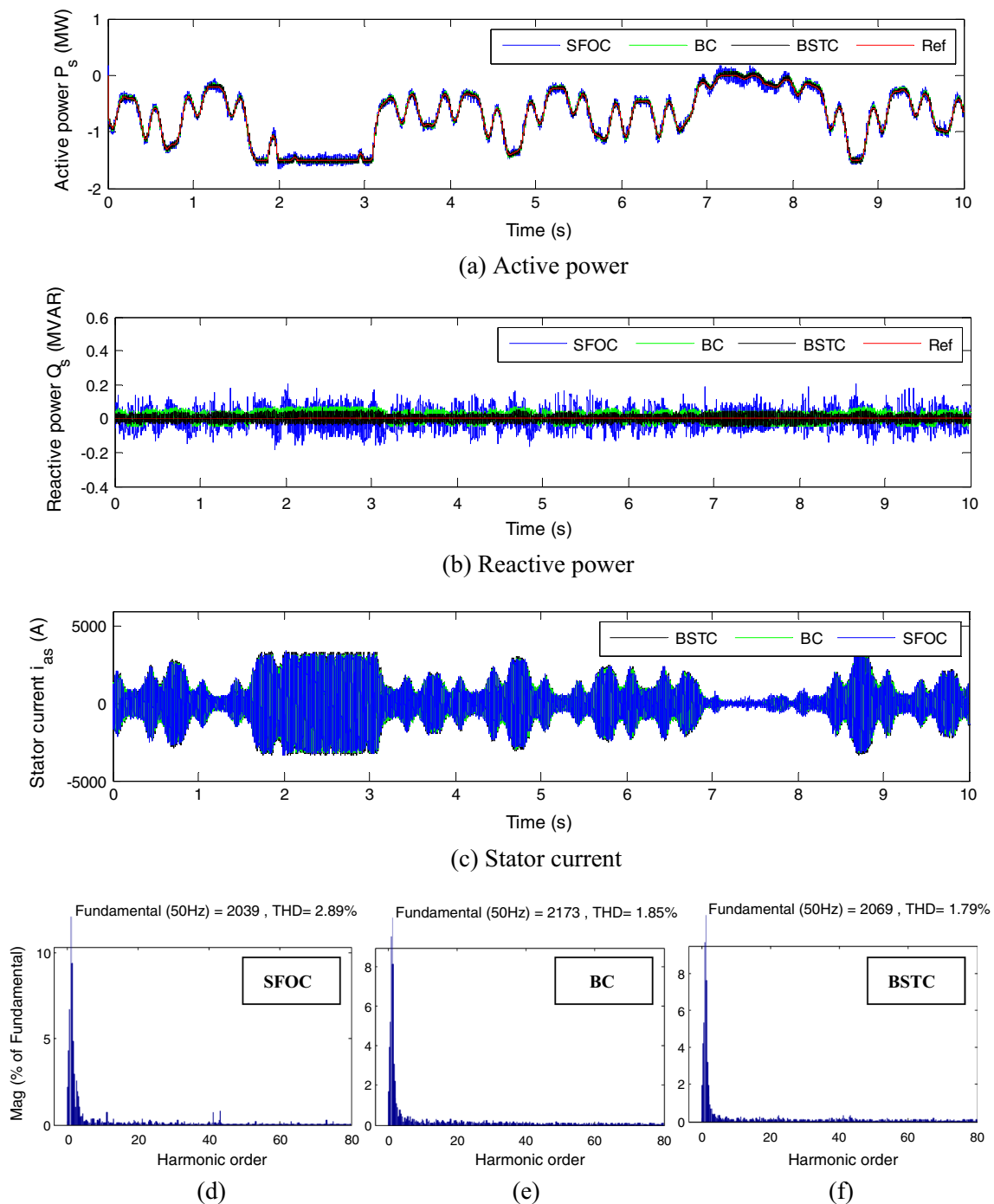


Fig. 19 Fourth test results

The objective of this test is to investigate how the behavior of BSTC compares to that of SFOC and BC. The results of this assessment are depicted in Figs. 19 and 20, along with Table 3. Upon reviewing Fig. 19, it is evident that both P_s and Q_s closely follow the reference values, with a notable advantage favoring the BSTC method in minimizing ripples. Additionally, active power experiences variations corresponding to changes in WS, while reactive power

remains unaffected by these fluctuations, maintaining a constant value of 0 MVAR throughout the simulation period, as depicted in Fig. 19a, b. Furthermore, the proposed BSTC demonstrates fewer ripples in both reactive and active powers, as illustrated in Fig. 20a, b.

Figure 19c depicts the stator current (i_{as}), and its variations are linked to changes in stator active power. Notably, there is a distinct advantage favoring BSTC in terms of ripple reduction

Fig. 20 Zoom of the fourth test results

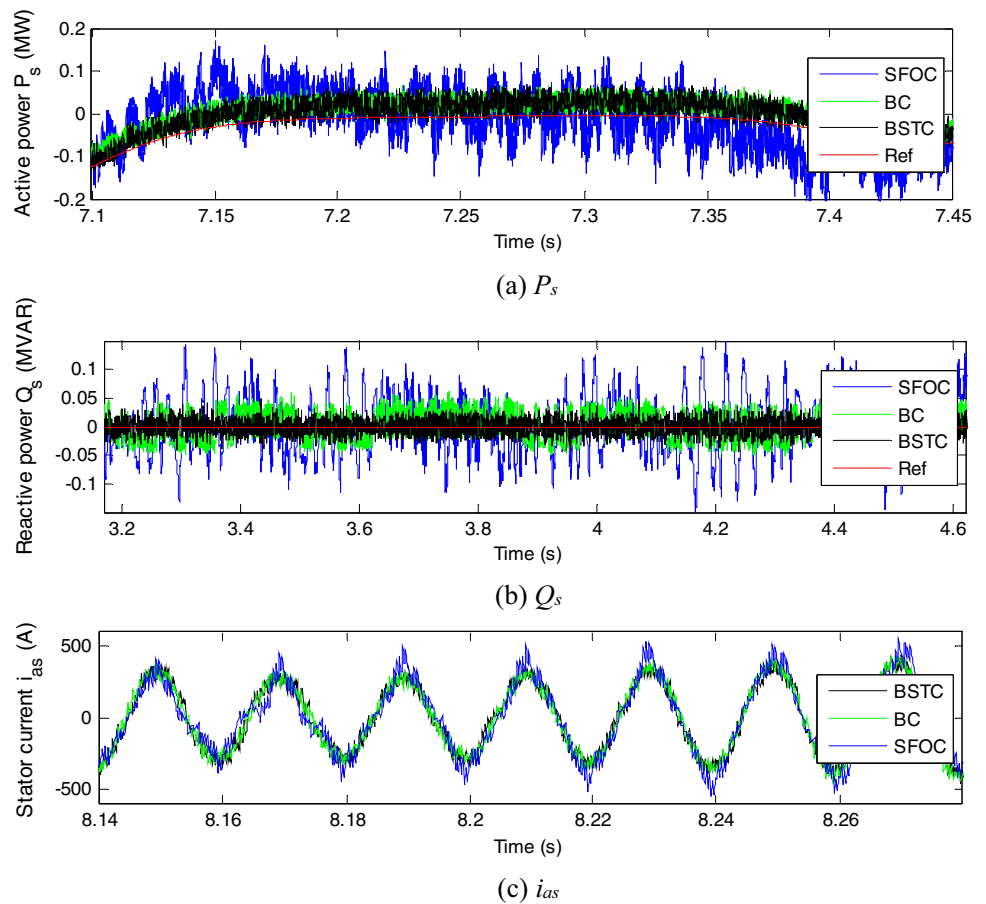


Table 3 Values and ratios of SSE in the fourth test case

	P_s (MW)	Q_s (MVAR)
SFOC	0.1135	0.1
BC	0.0635	0.06
BSTC	0.0278	0.038
Ratios (BSTC compared to SFOC)	75.50%	62%
Ratios (BSTC compared to BC)	56.22%	36.66%

when compared to the SFOC and BC techniques, as evident in Fig. 20c. Additionally, when BSTC is employed, the current waveform exhibits a high-quality sinusoidal shape, illustrated in Fig. 19d, e, f. These figures showcase the THD values of the current for SFOC, BC, and BSTC. The recorded THD values are 2.89% for SFOC, 1.85% for BC, and 1.79% for the proposed BSTC. It can be inferred that, in this test, the proposed control demonstrates the lowest THD of stator current. Consequently, employing the BSTC technique resulted in a THD reduction of approximately 38.06% compared to SFOC and 3.24% compared to BC.

Table 3 presents the numerical results of SSE in the fourth test. The table indicates that the recommended control

approach produced superior quantitative results compared to SFOC and BC. Specifically, the BSTC strategy led to significant reductions in SSE for active power, with percentages of 75.50% and 56.22% compared to SFOC and BC, respectively. In terms of reactive power, the proposed strategy achieved SSE reductions of 62% and 36.66% compared to SFOC and BC, respectively.

A comparative analysis between the suggested approach (BSTC) and the conventional ones (SFOC and BC) is presented in Table 4. Through this table, it can be noted that very good results are achieved, such as: an improvement in the quality of the current produced, perfect reactive and active stator power tracking, reduction of electromagnetic torque and stator power ripples, high precision, low rise time, negligible overshoot, short settling time, fast dynamic response and excellent robustness with the proposed approach. Moreover, the effect of grid voltage drop scenarios is relatively lower with the proposed approach than with the conventional ones.

At the end of this research work, we present a comparison between the suggested BSTC approach and some scientifically published works regarding the percentage of the stator current THD values. The results are illustrated in Table 5. According to this table, it can be observed that the BSTC

Table 4 Comparative study between the proposed technique and conventional ones

Performance criteria	Conventional methods		Proposed method (BSTC)
	SFOC	BC	
Stator powers undulations	High	Medium	Relatively low
Powers tracking	Good	Good	Excellent
Electromagnetic torque ripples	High	Medium	Relatively low
Quality of power	Low	Low	High
Overshoot	Remarkable	Neglected	Neglected
Rise time	Medium	Low	Low
Settling time	Medium	Low	Low
Precision	Medium	Medium	High
Robustness	Low	Good	Excellent
Grid voltage drop effect	High	Medium	Relatively low
Dynamic response	Medium	Fast	Fast
PI controller	Yes	No	No
Hybrid controller	No	No	Yes
STA utilization	No	No	Yes
THD of stator current	High	Medium	Relatively low
PWM	Yes	Yes	Yes
MPPT	Yes	Yes	Yes

Table 5 Comparative results between some scientific published articles and the proposed BSTC strategy in terms of the stator current THD

Reference	Control method	THD (%)
[37]	SMC	3.13
	SOSMC based on STA	2.62
[39]	Fuzzy SMC	2.85
[40]	SMC-DPC	1.66
[41]	Direct FOC with third-order sliding mode	1.42
[42]	DFOC	1.45
[43]	DPC using LCL-filter	4.05
[44]	DPC-PD(1+PI)	0.62
Proposed control	BSTC	0.54

strategy yielded much lower percentages of the stator current THD than other published control methods, such as direct field-oriented control (DFOC), SMC, Fuzzy SMC, SOSMC based on STA, direct power control (DPC) using an LCL-filter, DPC-PD(1+PI), and direct FOC with third-order sliding mode. Finally, it can be said that the BSTC method proposed in this research work provides a good representation of sinusoidal current.

7 Conclusion

This research work was presented a robust BSTC strategy for a DFIG-based DRWT under normal operating conditions and grid voltage drop scenarios. The proposed control strategy combines the conventional BC and STA to enhance the quality of electrical energy produced by the DFIG-based DRWT. By employing the Lyapunov function method, the control laws of the BSTC strategy are derived, ensuring the system's convergence and stability. Extensive simulation tests conducted using MATLAB software, including RTT, RT, GVDT, and random wind speed test, demonstrate the effectiveness of the suggested control.

The results indicate significant improvements compared to conventional control methods such as BC and SFOC. The BSTC strategy effectively mitigates the coupling effect, reduces stator power undulations, and exhibits high robustness. Additionally, the suggested controller achieves a low THD value in stator current when compared to some published controls.

Notably, under grid voltage drop conditions, the proposed BSTC strategy outperforms SFOC and BC by reducing ripples in electromagnetic torque. Consequently, this helps to lower winding losses and alleviate excessive shaft stress. Furthermore, the results indicate that the BSTC led to a 57.14% reduction in THD compared to SFOC and a 33.33% reduction compared to BC in the first test. On the other hand, in the second test, the proposed control minimizes the THD of the stator current by 63.29% compared to SFOC and by 40.20% compared to BC.

Finally, the BSTC strategy proves to be an effective solution for stator power regulation in DFIG-based DRWT systems. Its ability to address various operational conditions and deliver superior performance makes it a promising and practical control approach for enhancing the efficiency and reliability of renewable energy generation from wind turbines.

In future research, we will experimentally validate these findings and compare the results with existing studies. Additionally, we will implement novel strategies to control the studied system and achieve superior quality.

Declarations

Conflict of interest The authors declare that they have no known competing financial interests or personal relationships that could have appeared to influence the work reported in this paper.

References

- Shen, W.Z.; Yunakov, N.; Cao, J.F.; Zhu, W.J.: Development of a general sound source model for wind farm application. *Renew. Energy* **198**, 380–388 (2022). <https://doi.org/10.1016/j.renene.2022.07.161>
- Hussain, J.; Mishra, M.K.: An efficient wind speed computation method using sliding mode observers in wind energy conversion system control applications. *IEEE Trans. Ind. Appl.* **56**(1), 730–739 (2020). <https://doi.org/10.1109/TIA.2019.2942018>
- Neagoe, M.; Saulescu, R.: Comparative energy performance analysis of four wind turbines with counter-rotating rotors in steady-state regime. *Energy Rep.* **8**, 1154–1169 (2022). <https://doi.org/10.1016/j.egy.2022.07.092>
- Bai, H.; Wang, N.; Wan, D.: Numerical study of aerodynamic performance of horizontal axis dual-rotor wind turbine under atmospheric boundary layers. *Ocean Eng.* **280**, 114944 (2023). <https://doi.org/10.1016/j.oceaneng.2023.114944>
- Benbouhenni, H.; Colak, I.; Bizon, N.; Gheorghita Mazare, A.; Thounthong, P.: Direct vector control using feedback PI controllers of a DPAG supplied by a two-level PWM inverter for a multi-rotor wind turbine system. *Arab. J. Sci. Eng.* (2023). <https://doi.org/10.1007/s13369-023-08035-w>
- Verma, P.; Seethalekshmi, K.; Dwivedi, B.: A self-regulating virtual synchronous generator control of doubly fed induction generator-wind farms. *IEEE Can. J. Electr. Comput. Eng.* **46**(1), 35–43 (2023). <https://doi.org/10.1109/ICJECE.2022.3223510>
- Emerson, L.S.; Cursino, B.J.; Victor Felipe, M.B.M.; Nady, R.; da Silva, E.R.C.: Dual converter connecting open-end doubly fed induction generator to a DC-microgrid. *IEEE Trans. Ind. Appl.* **57**, 5001–5012 (2021). <https://doi.org/10.1109/TIA.2021.3087119>
- Lingling, F.; Haiping, Y.; Zhixin, M.: A novel control scheme for DFIG-based wind energy systems under unbalanced grid conditions. *Electr. Power Syst. Res.* **81**(2), 254–262 (2011). <https://doi.org/10.1016/j.epsr.2010.08.011>
- Guillermo, N.G.; Cristian, H.D.A.; Diego, A.A.: A control strategy for DFIG-based systems operating under unbalanced grid voltage conditions. *Int. J. Electr. Power Energy Syst.* **142**, 108273 (2022). <https://doi.org/10.1016/j.ijepes.2022.108273>
- Elmostafa, C.; Youssef, E.; Abdellatif, O.; Smail, S.: Self-adapting PI controller for grid-connected DFIG wind turbines based on recurrent neural network optimization control under unbalanced grid faults. *Electr. Power Syst. Res.* **214**, 108829 (2023). <https://doi.org/10.1016/j.epsr.2022.108829>
- Susperregui, A.; Martinez, M.I.; Tapia-Otaegui, G.; Etxeberria, A.: Sliding-mode control algorithm for DFIG synchronization to unbalanced and harmonically distorted grids. *IEEE Trans. Sustain. Energy* **13**(3), 1566–1579 (2022). <https://doi.org/10.1109/TSTE.2022.3166217>
- Xiaobing, K.; Xuan, W.; Mohamed, A.A.; Xiangjie, L.; Kwang, Y.L.: Nonlinear MPC for DFIG-based wind power generation under unbalanced grid conditions. *Int. J. Electr. Power Energy Syst.* **134**, 107416 (2022). <https://doi.org/10.1016/j.ijepes.2021.107416>
- Rostami, M.; Madani, S.M.; Ademi, S.: Sensorless closed-loop voltage and frequency control of stand-alone dfigs introducing direct flux-vector control. *IEEE Trans. Industr. Electron.* **67**(7), 6078–6088 (2020). <https://doi.org/10.1109/TIE.2019.2955421>
- Ramu, N.; Narayanan, G.: Stator flux based model reference adaptive observers for sensorless vector control and direct voltage control of doubly-fed induction generator. *IEEE Trans. Ind. Appl.* **56**(4), 3776–3789 (2020). <https://doi.org/10.1109/TIA.2020.2988426>
- Yahdou, A.; Belhadj, D.A.; Boudjema, Z.; Mehedi, F.: Improved vector control of a counter-rotating wind turbine system using adaptive backstepping sliding mode. *J. Eur. des Syst. Autom.* **53**(5), 645–651 (2020). <https://doi.org/10.18280/jesa.530507>
- Fateh, M.; Abdellatif, R.: Comparative study of integral and classical backstepping controllers in IFOC of induction motor fed by voltage source inverter. *Int. J. Hydrog. Energy* **42**(28), 17953–17964 (2017). <https://doi.org/10.1016/j.ijhydene.2017.04.292>
- Mai, T.; Tran, H.: An adaptive robust backstepping improved control scheme for mobile manipulators robot. *ISA Trans.* **137**, 446–456 (2023). <https://doi.org/10.1016/j.isatra.2023.01.005>
- Guettab, A.; Bounadja, E.; Boudjema, Z.; Taleb, R.: Third-order super-twisting control of a double stator asynchronous generator integrated in a wind turbine system under single-phase open fault. *Int. J. Circuit Theory Appl.* **51**(4), 1858–1878 (2023). <https://doi.org/10.1002/cta.3511>
- Jesus, L.F.; Juárez-Abad, J.A.; Arturo, H.M.; Castro-Heredia, O.; Guerrero-Castellanos, J.F.; Heredia-Barba, R.; Curiel-Olivares, G.: Sliding mode control based on linear extended state observer for DC-to-DC buck-boost power converter system with mismatched disturbances. *IEEE Trans. Ind. Appl.* **58**(1), 940–950 (2022). <https://doi.org/10.1109/TIA.2021.3130017>
- Tahir, K.; Allaoui, T.; Denai, M.; Mekhilef, S.; Belfedal, C.; Doumi, M.: Second-order sliding mode control of wind turbines to enhance the fault-ride through capability under unbalanced grid faults. *Int. J. Circuit Theory Appl.* **49**(7), 1959–1986 (2021). <https://doi.org/10.1002/cta.3023>
- Ding, S.; Li, S.; Zheng, W.X.: New approach to second-order sliding mode control design. *IET Control Theory Appl.* **7**(18), 2188–2196 (2013). <https://doi.org/10.1049/iet-cta.2013.0394>
- Li, F.; Du, C.; Yang, C.; Gui, W.: Passivity-based asynchronous sliding mode control for delayed singular markovian jump systems. *IEEE T Automat. Contr.* **63**(8), 2715–2721 (2018)
- Fujimoto, K.; Sakata, N.; Maruta, I.; Ferguson, J.: A passivity based sliding mode controller for simple port-hamiltonian systems. *IEEE Control Syst. Lett.* **5**(3), 839–844 (2021). <https://doi.org/10.1109/LCSYS.2020.3005327>
- Chen, C.; Yu, H.: Backstepping sliding mode control of induction motor based on disturbance observer. *IET Electr. Power App.* **14**(12), 2537–2546 (2020)
- Hu, W.; Ding, F.; Zhang, J.; Zhang, B.; Zhang, N.; Qin, A.: Robust adaptive backstepping sliding mode control for motion mode decoupling of two-axle vehicles with active kinetic dynamic suspension systems. *Int. J. Robust Nonlinear Control* **30**(8), 3110–3133 (2020)
- Zhang, X.; Huang, W.; Wang, Q.G.: Robust H_∞ adaptive sliding mode fault tolerant control for T-S Fuzzy fractional order systems with mismatched disturbances. *IEEE T Circuits Syst.* **68**(3), 1297–1307 (2021)
- He, L.; Wang, F.; Ke, D.: FPGA-based sliding-mode predictive control for PMSM speed regulation system using an adaptive ultralocal model. *IEEE Trans. Power Electr.* **36**(5), 5784–5793 (2021)
- Huang, C.; Naghdy, F.; Du, H.: Fault tolerant sliding mode predictive control for uncertain steer-by-wire system. *IEEE Trans. Cybernetics* **49**(1), 261–272 (2019)
- Ali, S.; Prado, A.; Pervaiz, M.: Hybrid backstepping-super twisting algorithm for robust speed control of a three-phase induction motor. *Electronics* **12**, 681 (2023). <https://doi.org/10.3390/electronics12030681>



30. Benbouhenni, H.; Mehedi, F.; Soufiane, L.: New direct power synergetic-SMC technique based PWM for DFIG integrated to a variable speed dual-rotor wind power. *Automatika* **63**(4), 718–731 (2022)
31. Farahani, E.M.; Hosseinzadeh, N.; Ektesabi, M.: Comparison of fault-ride-through capability of dual and single-rotor wind turbines. *Renew. Energy* **48**, 473–481 (2012)
32. Boudjema, Z.; Taleb, R.; Djeriri, Y.; Yahdou, A.: A novel direct torque control using second order continuous sliding mode of a doubly fed induction generator for a wind energy conversion system. *Turk. J. Electr. Eng. Comput. Sci.* **25**(2), 965–975 (2017). <https://doi.org/10.3906/elk-1510-89>
33. Abdeddaim, S.; Betka, A.: Optimal tracking and robust power control of the DFIG wind turbine. *Int. J. Electr. Power Energy Syst.* **49**, 234–242 (2013). <https://doi.org/10.1016/j.ijepes.2012.12.014>
34. Yahdou, A.; Belhadj, D.A.; Boudjema, Z.; Mehedi, F.: Using adaptive second order sliding mode to improve power control of a counter-rotating wind turbine under grid disturbances. *Eur. J. Electr. Eng.* **22**(6), 427–434 (2020). <https://doi.org/10.18280/ejee.220604>
35. Hiremath, R.; Moger, T.: Modified super twisting algorithm based sliding mode control for LVRT enhancement of DFIG driven wind system. *Energy Rep.* **8**, 3600–3613 (2022). <https://doi.org/10.1016/j.egy.2022.02.235>
36. Boyette, A.; Saadate, S.; Poure, P.: Direct and indirect control of a Doubly Fed Induction Generator wind turbine including a storage unit. In: *IECON 2006—32nd Annual Conference on IEEE Industrial Electronics*, Paris, (2006). <https://doi.org/10.1109/IECON.2006.347300>
37. Yahdou, A.; Hemici, B.; Boudjema, Z.: Second order sliding mode control of a dual-rotor wind turbine system by employing a matrix converter. *J. Electr. Eng.* **16**, 11 (2016)
38. Farahani, E.M.; Hosseinzadeh, N.; Ektesabi, M.: Comparison of dynamic responses of dual and single rotor wind turbines under transient conditions. In: *IEEE International Conference on Sustainable Energy Technologies (ICSET)*, Kandy, (2010). <https://doi.org/10.1109/ICSET.2010.5684946>
39. Boudjema, Z.; Meroufel, A.; Djerriri, Y.; Bounadja, E.: Fuzzy sliding mode control of a doubly fed induction generator for energy conversion. *Carpathian J. Electr. Comput. Eng.* **6**(2), 7–14 (2013)
40. Yaichi, I.; Semmah, A.; Wira, P.; Djeriri, Y.: Super-twisting sliding mode control of a doubly-fed induction generator based on the SVM strategy. *Period. Polytech. Electr. Eng. Comput. Sci.* **63**(3), 178–190 (2019). <https://doi.org/10.3311/PPee.13726>
41. Benbouhenni, H.; Bizon, N.: Third-order sliding mode applied to the direct field-oriented control of the asynchronous generator for variable-speed contra-rotating wind turbine generation systems. *Energies* **14**, 1–20 (2021). <https://doi.org/10.3390/en14185877>
42. Benbouhenni, H.; Bizon, N.: A synergetic sliding mode controller applied to direct field-oriented control of induction generator-based variable speed dual-rotor wind turbines. *Energies* **14**(15), 1–17 (2021). <https://doi.org/10.3390/en14154437>
43. Alhato, M.M.; Bouallègue, S.: Direct power control optimization for doubly fed induction generator based wind turbine systems. *Math. Comput. Appl.* (2019). <https://doi.org/10.3390/mca24030077>
44. Benbouhenni, H.; Bounadja, E.; Gasmi, H.; Bizon, N.; Colak, I.: A new PD(1+PI) direct power controller for the variable-speed multi-rotor wind power system driven doubly-fed asynchronous generator. *Energy Rep.* **8**, 15584–15594 (2022). <https://doi.org/10.1016/j.egy.2022.11.136>

Springer Nature or its licensor (e.g. a society or other partner) holds exclusive rights to this article under a publishing agreement with the author(s) or other rightsholder(s); author self-archiving of the accepted manuscript version of this article is solely governed by the terms of such publishing agreement and applicable law.